Phosphorus-doped reduced graphene oxide as an electrocatalyst counter electrode in dye-sensitized solar cells

Zegao Wang, Pingjian Li*, Yuanfu Chen*, Jiarui He, Jingbo Liu, Wanli Zhang, Yanrong Li

State Key Laboratory of Electronic Thin Films and Integrated Devices, University of Electronic Science and Technology of China, Chengdu 610054, PR China

HIGHLIGHTS

- Phosphorus (P)-doped rGO was synthesized with two bonding states of P–C and P–O.
- For the first time, P-doped rGO is employed as the counter electrode (CE) in DSSC.
- P doping can effectively enhance the electrocatalytic activity of rGO.
- P–C structures have higher electrocatalytic activity than P–O ones.
- P-doped rGO shows comparable electrocatalytic activity to Pt as CE.

ARTICLE INFO

ABSTRACT

In this study, phosphorus (P) atoms were doped into reduced graphene oxide (rGO) with two bonding states of P–C and P–O by using annealing treatment. For the first time, the P-doped rGO (PrGO) was employed as the counter electrode (CE) for dye-sensitized solar cell (DSSC). The electrochemical studies reveal that the P doping can effectively enhance the electrocatalytic activity of rGO, and P–C structures have higher electrocatalytic activity than P–O ones for I^-/I_3^- redox reaction. More significantly, PrGO shows comparable electrocatalytic ability to Pt as CEs. It therefore seems promising for PrGO to be widely used in metal-free DSSCs with low cost and high efficiency.

© 2014 Elsevier B.V. All rights reserved.

1. Introduction

Due to the low cost, simple fabrication process and reasonable conversion efficiency, dye-sensitized solar cells (DSSCs) have received much attention [1–4]. A typical DSSC consists of three components: a dye-sensitized TiO_2 photoanode, an I^-/I_3^- electrolyte and a counter electrode (CE). Commonly, Pt films on the conductive glass were employed as CE materials, which have high electrical conductivity and electrocatalytic ability for I^-/I_3^- redox reaction [1–4]. However, due to the high cost of Pt, it is significant to develop cheap CE materials for DSSCs with high conversion efficiencies.

So far, various carbonaceous materials, conductive polymers and inorganic compounds have been proposed as cheap CE materials for DSSCs [5–9]. Among them, reduced graphene oxide (rGO), one kind of carbonaceous materials, has attracted considerable attention due to its remarkable electrical, optical, and mechanical properties as well as its extraordinarily high surface area [10–12]. Several groups have reported that the DSSCs employing rGO CEs have high conversion efficiencies [3,4,12,13]. Thus, it is significant to investigate the electrochemical properties of rGO and further enhance its electrocatalytic activity for I^-/I_3^- redox reaction.

Recently, many reports have demonstrated that heteroatom doping can effectively modulate the electron structure and improve the electrochemical properties of rGO. For example, nitrogen (N), boron (B) and sulfur (S) atoms doped into graphene can enhance the electrical conductivity and electrocatalytic activity of rGO, which can be used as electrode materials of supercapacitors [14–16], Li-ions batteries [17,18], fuel cells (oxygen reduction reaction) [19–22] and DSSCs [23–26] with high performances. Most recently, phosphorus-doped rGO (PrGO) was synthesized and further used as electrode materials for supercapacitors [27], fuel cells [28,29] and Li-ions batteries [29]. However, to the best of our knowledge, the application of PrGO as metal-free CEs in DSSCs has not been explored.

In this study, PrGO was synthesized by annealing a mixture of graphene oxide (GO) and triphenylphosphine, which were

* Corresponding authors.
E-mail addresses: lipingjian@uestc.edu.cn (P. Li), yfchen@uestc.edu.cn (Y. Chen).

employed as the carbon and phosphorus (P) sources, respectively. For the first time, the PrGO was used as the CE for DSSC. It shows remarkable catalytic activity, which can be comparable to the Pt CE. We have systematically investigated the electrocatalytic mechanism of PrGO for I^-/I_3^- redox reaction. The studies reveal that P doping can effectively enhance the catalytic activity of rGO, and the P–C structures have higher catalytic activity than P–O ones.

2. Experimental

2.1. Synthesis of PrGO

GO was synthesized from flake graphite (Qingdao Tianhe Graphite Co. Ltd., Qingdao, China) by a modified Hummers method [30]. To synthesize PrGO, 1 g GO and 1 g triphenylphosphine were first ultrasonically dispersed in ethanol for 30 min, and then spread onto an evaporating dish and dried, forming a uniform solid mixture. And then, the mixture was placed into a quartz tube and annealed at 600–1000 °C for 30 min with argon and hydrogen. The flux of argon and hydrogen were both 500 sccm. Finally, the PrGO was obtained by collecting and washing several times. For comparison, the undoped rGO was synthesized by the same procedure except that the triphenylphosphine (P source) was absent. The as-synthesized PrGO and rGO samples are denoted as PrGOX and rGOX, respectively, where X represents the annealing temperature (°C).

2.2. Fabrication of PrGO and rGO CEs

The PrGO (or rGO) CE was fabricated as follows. First, 90 wt% PrGO (or rGO) and 10 wt% polyvinylidene fluoride (PVDF) were dispersed in N-Methyl-2-pyrrolidone (NMP) by using an ultrasonic horn, and then a layer of paste was coated on fluorine-doped tin oxide glass plates. The CEs were heated in vacuum at 120 °C overnight. The size of CE was 1 cm². For comparison, 100 nm Pt film sputtered on FTO was employed as the Pt CE.

2.3. Fabrication of DSSCs

The DSSC was made of a photoanode, a CE and a DHS-E23 electrolyte solution. The TiO₂ photoanode, N719 and DHS-E23 were purchased from Co. Ltd. Dalian Heptachroma SolarTech. The TiO₂ photoanode was sensitized by immersing into an ethanol solution containing the 0.5 mM N719 dye solution for 12 h. The area of TiO₂ photoanode was 0.36 cm².

2.4. Characterization

The transmission electron microscopy (TEM) and scanning transmission electron microscopy (STEM) images were taken with an FEI Tecnai G2 microscope. XPS was performed on a Kratos XSAM800 using Al Ka radiation (144 W, 12 mA, 12 kV). The photocurrent density–voltage characteristics of DSSCs were measured using a Keithley-2000 and Yokogawa-7651 source meters under the excitation of 100 mW cm⁻² AM 1.5 white light from a solar simulator (XQ350W, Shanghai Lansheng Electronic Co., Ltd). Cyclic voltammetry (CV) measurements were conducted, in which an as-prepared CE was taken as the working electrode in the two-electrode one-compartment cell and the Pt sheet was simultaneously served as both the reference electrode and counter electrode in an acetonitrile solution with 10 mM LiI, 1 mM I₂, and 0.1 M LiClO₄. The electrochemical impedance spectroscopy (EIS) measurements were performed in the frequency range of 0.1 Hz–1 MHz in a two-electrode system on an electrochemical workstation (CHI660D, Chenhua Instruments Co., Shanghai).

3. Results and discussions

Fig. 1(a) shows a typical TEM image of PrGO900. The image reveals transparent graphene sheets with wrinkle and fold features, which may originate from defective structures formed during the P doping and reduction process of GO. The corresponding EDX spectrum (Fig. 1(b)) confirms the presence of P atoms in PrGO900 (The Si peak in Fig. 1(b) originates from the Si (Li) detectors). Fig. 1(c)–(e) represent the STEM elemental mappings of PrGO900. The similar C and P mappings reveal that the doped P atoms are homogenously distributed in the plane of graphene.

In order to further confirm the P doing and investigate the bonding configurations of P atoms in PrGO, the XPS measurements were performed at room temperature. As shown in Fig. 2(a), the P peak appears and the intensity of O peak decreases in the XPS spectrum of PrGO900 compared to GO. It indicates that the P atoms
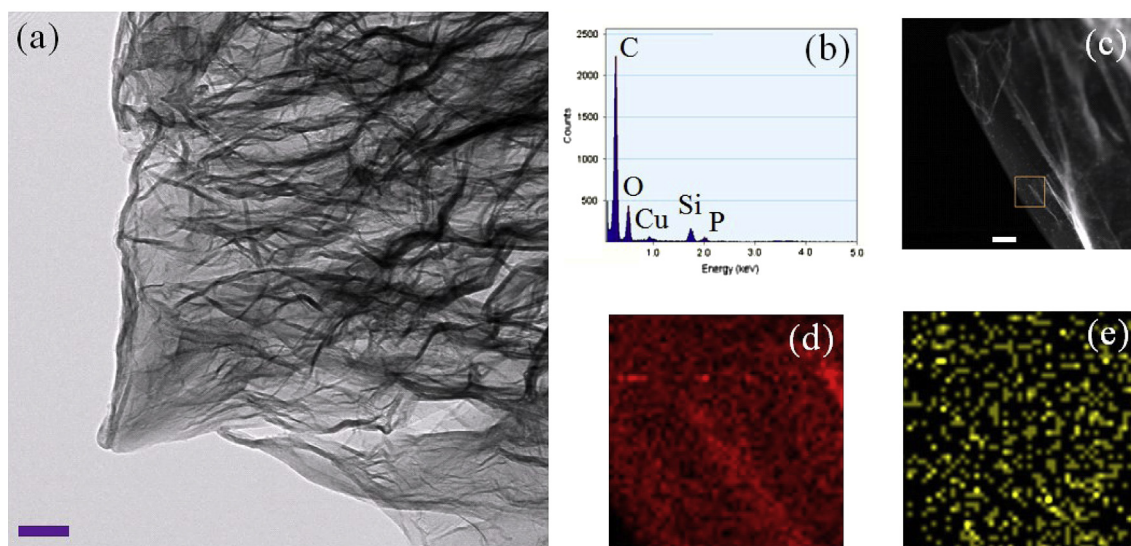

Fig. 1. (a–c) TEM image, EDX spectrum and STEM image of PrGO900, respectively. (d) C- and (e) P-elemental mapping of orange square region in (c). The scale bars in (a) and (c) are both 100 nm.
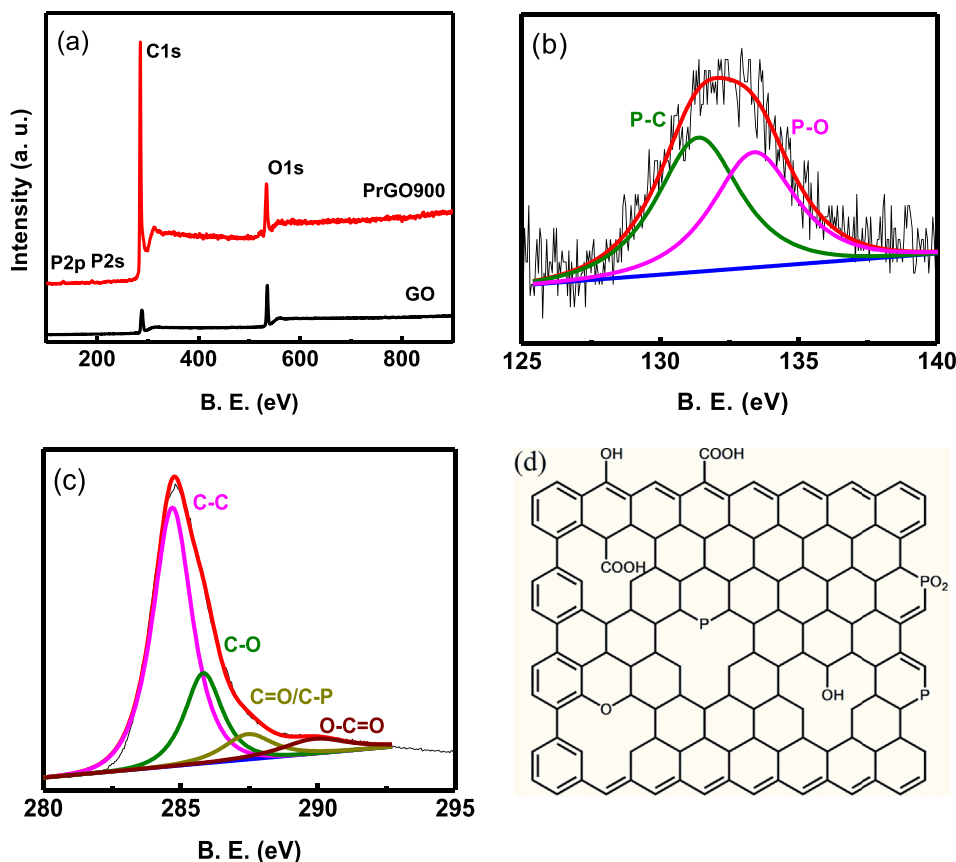
Fig. 2. (a) XPS spectra of GO and PrGO900. High resolution (b) P2p and (c) C1s XPS spectrum of PrGO900. (d) Schematic structure of PrGO.

are incorporated into rGO and the large amounts of oxygen-functional groups (C—O bonds, carbonyls or carboxylates) on GO are removed during the annealing treatment. It is noted that possibility of physical adsorption of P onto the samples is excluded by the flowing reason. The samples were ultrasonically dispersed in various solvents like ethanol, acetone, ether and H_2O; the XPS results reveal no change in the P level before and after sonication (XPS data not shown).

Fig. 2(b) is the high resolution P2p XPS spectrum of PrGO900. The P2p peak can be deconvoluted into two peaks at binding energies of ∼131.2 and ∼133.4 eV, which correspond to the P—C and P—O energy positions, respectively [28,29,31]. Fig. 2(c) shows the high resolution C1s spectrum of PrGO900. The C1s peak can be deconvoluted into four peaks at binding energies of ∼284.7, ∼285.8, ∼287.5 and ∼289.9 eV, which correspond to C—C, C—O, C=O(C—P) and O—C=O, respectively. Note that the peak of C=O is overlaid with C—P, which is similar with the overlay of C=O and C—N peaks in N-doped rGO [32]. In addition, the P/C ratio (P—C and P—O) of PrGO900 is 1.27 at%, which is comparable to previous reports [28,29].

In order to investigate the P doping and GO reduction mechanisms, we have studied the influence of annealing temperature on the elemental composition of PrGO by XPS analysis. The high resolution P2p XPS spectra of PrGO synthesized at different annealing temperature were shown in Fig. S1 (see Supplementary materials). When the annealing temperature is 600 °C, there is only one peak corresponding to P—O bond. When the annealing temperature is larger than 600 °C, a new peak, corresponding to P—C bond, appears.

Fig. 3(a) shows the P/C ratio in PrGO synthesized at different annealing temperature. The total P/C ratio is 1.07, 1.10, 1.27 and 1.08 at% for PrGO600, PrGO800, PrGO900 and PrGO1000, respectively. When the annealing temperature increases from 600 to 1000 °C, the P—O/C ratio decreases from 1.07 to 0.47 at%, while the P—C/C ratio increases from 0 to 0.61 at%. When the annealing temperature is 900 °C, the total P/C ratio reaches a maximum value of 1.27 at%. The above data shows that P—C bonds can be easier formed than P—O bonds at higher annealing temperature. It is attributed that P—O bonds are not thermally stable at higher annealing temperature, which is similar with previous report for the breakage of N—O bonds in N-doped graphene caused by overheating [33,34].

For further investigating the effect of P doping on the degree reduction of GO, we have studied the O/C ratio of PrGO and rGO synthesized at different annealing temperature, as shown in Fig. 3(b). The O/C ratio of PrGO is obviously smaller than rGO at the same annealing temperature. It therefore seems that the P doping preferably occurs at the sites of oxygen functional groups in GO, thus affording a more effective reduction of GO. This phenomenon is similar to the case of N and S doping and reduction of GO [33–35].

To investigate the influence of P doping on the electrocatalytic properties of rGO, we have comparatively studied the photovoltaic performance of DSSCs employing rGO, PrGO and Pt as CE materials. To avoid the test error, 8 different samples for each type CE material were fabricated and measured. Fig. 4(a) shows the typical photocurrent density *vs* voltage characteristics of DSSCs employing rGO600, rGO800, rGO900 and rGO1000 CEs. As shown in Fig. 4(c), the conversion efficiencies of these DSSCs increase from ∼3.49% to ∼4.18% with increasing the annealing temperature from 600 to 1000 °C. The possible reason is that when the annealing temperature increases, oxygen-functional groups are removed, which
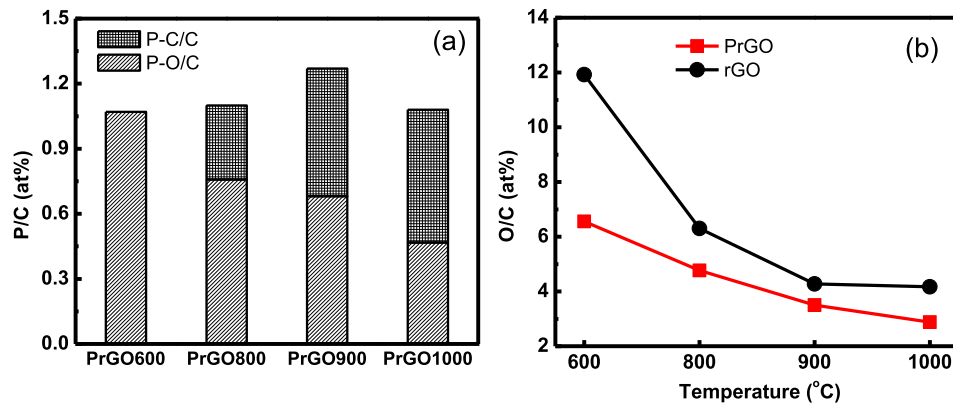
Fig. 3. The investigations of elemental compositions of PrGO and rGO synthesized at different annealing temperature by XPS analysis. (a) P and (b) O content as a function of annealing temperature.

simultaneously producing more topological defects with high electrocatalytic activity [36–38].

Fig. 4(b) shows the photovoltaic properties of DSSCs employing Pt, PrGO600, PrGO800, PrGO900 and PrGO1000 CEs. From Figs. 4(c) and 3(a), we can get following conclusions: (1) the DSSCs employing PrGO CEs (4.98%–6.04%) have higher conversion efficiencies than those employing rGO CEs (3.49%–4.18%), which indicates that the P doping can effective enhance the electrocatalytic activity of rGO. (2) Compared PrGO600 (P–O/C: 1.07 at%) with PrGO1000 (P–O/C: 0.47 at%, P–C/C: 0.61 at%), the higher conversion efficiency for PrGO1000 CE means that the P–C structures have higher electrocatalytic activity than P–O ones. (3) For the P–C or P–O structures, the electrocatalytic activity increases with increasing the P content, which results in the increase of conversion efficiency. (4) When the total P content reaches the maximum value of 1.27 at% (PrGO900), the corresponding DSSC has the highest conversion efficiency ($\sim 6.04\%$), which is 90% of that employing Pt CE ($\sim 6.80\%$). It shows that the PrGO900 can be used as the promising CE material for DSSCs with low cost and high efficiency.

In order to further understand the reaction kinetics and electrocatalytic properties of PrGO, CV measurements were performed. Fig. 5(a) shows the typical CV curves of rGO900, PrGO900 and Pt CEs at the scan rate of 10 mV s^{-1}. It can be obviously observed one pair of reduction and oxidation peaks in all curves, which are attributed to the reduction reaction ($I_3^- + 2e^- \rightarrow 3I^-$) and oxidation reaction ($3I^- \rightarrow I_3^- + 2e^-$), respectively [23,24,26]. The higher reduction current density corresponds to the faster rate for I_3^- reduction [23]. Compared Fig. 5(b) with Fig. 4(c), we find that the

variation of reduction current density is consistent with conversion efficiency. (1) PrGO CEs have higher reduction current densities (1.15–1.64 mA cm^{-2}) than rGO CEs (0.53–1.02 mA cm^{-2}). It means that the P doping can effectively increase the rate of I_3^- reduction, which corresponds to the enhancement of electrocatalytic activity. (2) PrGO1000 CE (1.44 mA cm^{-2}) has higher reduction current density than PrGO600 CE (1.15 mA cm^{-2}), which means that the P–C structures have higher electrocatalytic activity than P–O ones. (3) For the P–C or P–O structures, increasing the P content causes the increase of reduction current density of PrGO CE, which corresponds to the increase of electrocatalytic activity. (4) The PrGO900 CE with highest P content has the highest reduction current density (~ 1.64 mA cm^{-2}), which is $\sim 92\%$ of that of Pt CE (~ 1.78 mA cm^{-2}). It means that the PrGO CE has a comparable electrocatalytic ability to Pt CE.

In order to further confirm the studies on the electrocatalytic properties of PrGO, EIS measurements were conducted. Fig. 6(a) shows the typical EIS spectra of Pt, rGO900, PrGO900 CEs, and the equivalent circuit model used for fitting the resultant impedance spectra is illustrated in the inset of Fig. 6(a). R_{ct} is the charge-transfer resistance at the CE/electrolyte interface for I_3^- reduction. The lower R_{ct} corresponds to the higher electrocatalytic activity, which is due to the less overpotential required for the electron transferring from the CE to the electrolyte [23]. By comparing Fig. 6(b) with Fig. 5(b) (or Fig. 4(c)), we can find that the variation of R_{ct} is consistent with reduction current density (or conversion efficiency). For example, the R_{ct} values of PrGO CEs (3.28–4.39 Ω cm^2) are lower than those of rGO CEs (6.98–13.01 Ω cm^2); the PrGO1000
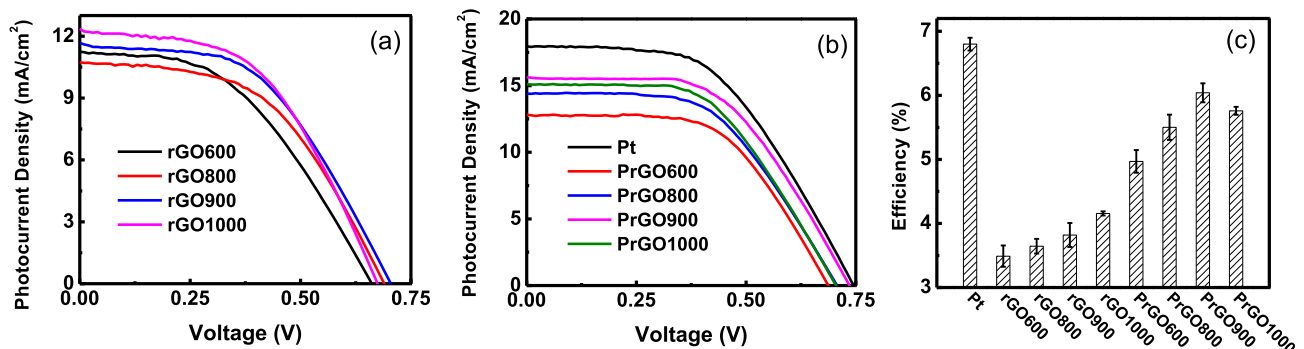

Fig. 4. (a) Typical photocurrent density–voltage characteristics of DSSCs employing rGO600, rGO800, rGO900 and rGO1000 CEs. (b) Typical photocurrent density–voltage characteristics of DSSCs employing Pt, PrGO600, PrGO800, PrGO900 and PrGO1000 CEs. (c) Conversion efficiency of DSSCs employing different CEs, and the values are mean and standard deviation (error bars) for 8 different samples.
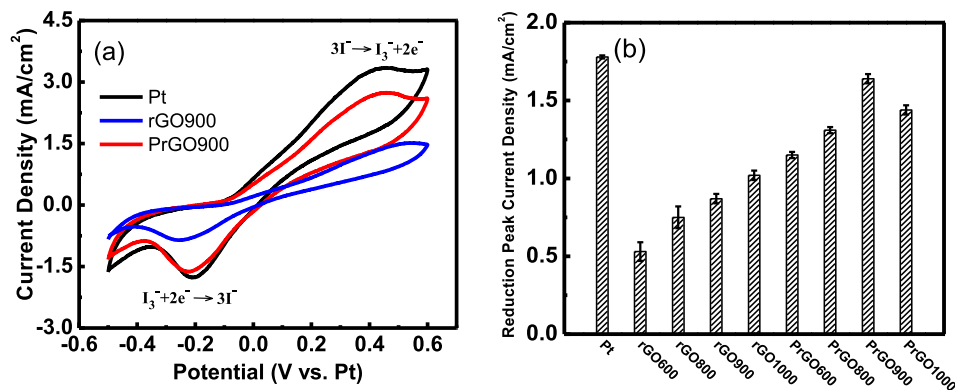
Fig. 5. (a) Typical CV curves of Pt, rGO900 and PrGO900 CEs at the scan rate of 10 mV s^{-1} in an acetonitrile solution with 10 mM LiI, 1 mM I$_2$ and 0.1 M LiClO$_4$. (b) Reduction peak current density of different CEs, and the values are mean and standard deviation (error bars) for 8 different samples.
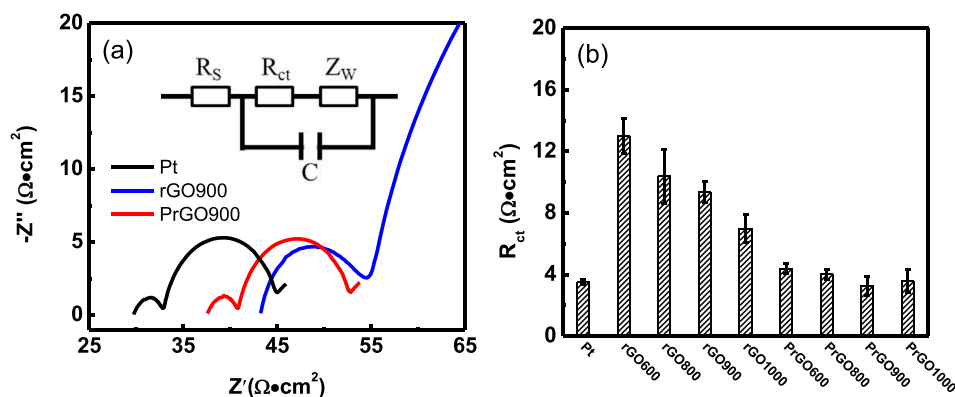

Fig. 6. (a) Typical EIS spectra of the dummy cell fabricated with two identical CEs. The inset is the equivalent circuit model for I$^-$/I$_3^-$ reaction. R_s: ohmic serial resistance; R_{ct}: charge-transfer resistance at the CE/electrolyte interface; C: double layer capacitance; Z_w: diffusion impedance. (b) R_{ct} of different CEs, and the values are mean and standard deviation (error bars) for 8 different samples.

CE (3.57 Ω cm^2) has lower R_{ct} than PrGO600 CE (4.39 Ω cm^2); the PrGO900 CE has the lowest value of R_{ct} (3.28 Ω cm^2), which is even lower than that of Pt CE (3.51 Ω cm^2). Thus, the photovoltaic, CV and EIS results all indicate that the P doping can effectively enhance the electrocatalytic ability of rGO for I$_3^-$ reduction, and P−C structures have higher electrocatalytic activity than P−O ones. More significantly, PrGO CEs have shown promising potential for DSSCs with low cost and high efficiency.

Furthermore, the effect mechanism of P doping on the electrocatalytic properties of rGO was discussed. Based on the previous studies on the electrocatalytic mechanism of N-doped rGO, the enhancing electrocatalytic activity of rGO caused by P doping may be attributed to the following three reasons. (1) The electronegativity of P atom is 2.1, which is smaller than that of carbon atom (2.5). Thus, the compensating positive charge is distributed on the doped P atom, which can readily attract I$_3^-$ ion and electrons from the anode, thus promoting the I$_3^-$ reduction [39,40]. (2) The conjugation effect of the lone pair electrons on the P atoms and graphene π-system may reduce the barrier for I$_3^-$ reduction, which is similar with the enhancing ORR activity of N-doped rGO caused by N doping [41−43]. (3) The doped P atoms (P−C or P−O) are usually located at edge or defects sites, which are chemically active themselves [21,44−47]. However, the more exact mechanism need to be further studied in future. In addition, for the P−C and P−O structures, the lower electrocatalytic activity for P−O structures may be attributed that the O atoms weakens the interaction effect of P and carbon atoms in PrGO.

4. Conclusions

In summary, we have synthesized PrGO by using annealing treatment, in which GO and triphenylphosphine were employed as the carbon and P sources, respectively. The TEM and XPS studies show that the P atoms are incorporated into rGO with two bonding states of P−C and P−O, and the P doping can effectively facilitate the GO reduction. Furthermore, we have employed PrGO as CE materials for DSSCs and investigated the electrocatalytic properties of PrGO CE. The photovoltaic, CV and EIS studies all reveal that PrGO CE has high electrocatalytic activity and the P doping can effectively enhance the electrocatalytic activity of rGO. Further studies have demonstrated that P−C structures have higher electrocatalytic activity than P−O ones. Finally, the highest conversion efficiency of DSSC employing PrGO CE is 6.25%, which is 90% of that employing Pt CE. It means that PrGO can be used as the promising CE material for DSSCs with low cost and high efficiency.

Appendix A. Supplementary data

Supplementary data related to this article can be found at http://dx.doi.org/10.1016/j.jpowsour.2014.03.118.

References

[1] H. Wang, Y.H. Hu, Energy Environ. Sci. 5 (2012) 8182–8188.
[2] B. Munkhbayar, Md. J. Nine, J. Jeoun, M. Ji, H. Jeong, H. Chung, J. Power Source 230 (2013) 207–217.
[3] J.D. Roy-Mayhew, D.J. Bozym, C. Punckt, I.A. Aksay, ACS Nano 4 (2010) 6203–6211.
[4] L. Kavan, J.H. Yum, M. Gratzel, ACS Nano 5 (2011) 165–172.
[5] J. Ma, L. Zhou, C. Li, J. Yang, T. Meng, H.M. Zhou, M.X. Yang, F. Yu, J.H. Cheng, J. Power Source 247 (2014) 999–1004.
[6] K.S. Lee, Y.B. Lee, J.Y. Lee, J.H. Ahn, J.H. Park, ChemSusChem 5 (2012) 379–382.
[7] V. Kwon, V. Ganapathy, Y.H. Kim, K.D. Song, H.G. Park, Y. Jun, P.J. Yoo, J.H. Park, Nanoscale 5 (2013) 7838–7843.
[8] M.R. Golobostanfard, H. Abdizadeh, Sol. Energy Mater. Sol. Cells 120 (2014) 295–302.
[9] F. Gong, X. Xu, Z.Q. Li, G. Zhou, Z.S. Wang, Chem. Commun. 49 (2013) 1437–1439.
[10] Z.G. Wang, Y.F. Chen, P.J. Li, X. Hao, J.B. Liu, R. Huang, Y.R. Li, ACS Nano 5 (2011) 7149–7154.
[11] K.H. Kim, M.H. Yang, K.M. Cho, Y.S. Jun, S.B. Lee, H.T. Jung, Sci. Rep. 3 (2013) 3251.
[12] S. Das, P. Sudhagar, E. Ito, D.Y. Lee, S. Nagarajan, S.Y. Lee, Y.S. Kang, W. Choi, J. Mater. Chem. 22 (2012) 20490–20497.
[13] J.E. Trancik, S.C. Barton, J. Hone, Nano Lett. 8 (2008) 982–987.
[14] Z.S. Wu, A. Winter, L. Chen, Y. Sun, A. Turchanin, X.L. Feng, K. Mullen, Adv. Mater. 24 (2012) 5130–5135.
[15] H.M. Jeong, J.W. Lee, W.H. Shin, Y.J. Choi, H.J. Shin, J.K. Kang, J.W. Choi, Nano Lett. 11 (2011) 2472–2477.
[16] L.L. Zhang, X. Zhao, H.X. Ji, M.D. Stoller, L.F. Lai, S. Murali, S. Mcdonnell, B. Cleveger, R.M. Wallace, R.S. Ruoff, Energy Environ. Sci. 5 (2012) 9618–9625.
[17] A.L.M. Reddy, A. Srivastava, S.R. Gowda, H. Gullapalli, M. Dubey, P.M. Ajayan, ACS Nano 4 (2010) 6337–6342.
[18] Z.S. Wu, W.C. Ren, L. Xu, F. Li, H.M. Chen, ACS Nano 5 (2011) 5463–5471.
[19] S.B. Yang, L.J. Zhi, K. Tang, X.L. Feng, J. Maier, K. Mullen, Adv. Funct. Mater. 22 (2012) 3634–3640.
[20] J. Liang, Y. Jiao, M. Jaroniec, S.Z. Qiao, Angew. Chem. Int. Ed. 51 (2012) 11496–11500.
[21] L.F. Lai, J.R. Potts, D. Zhan, L. Wang, C.K. Poh, C.H. Tang, H. Gong, Z.X. Shen, J.Y. Lin, R.S. Ruoff, Energy Environ. Sci. 5 (2012) 7936–7942.
[22] I. Jeon, H. Choi, M.J. Ju, I.T. Choi, K. Lim, J. Ko, H.K. Kim, J.C. Kim, J. Lee, D.B. Shin, S. Jung, J. Seo, M. Kim, N. Park, L.M. Dai, J. Baek, Sci. Rep. 3 (2013) 2260.
[23] G.Q. Wang, W. Xing, S.P. Zhuo, Electrochim. Acta 92 (2013) 269–275.
[24] Y.H. Xue, J. Liu, H. Chen, R.G. Wang, D.Q. Li, J. Qu, L.M. Dai, Angew. Chem. Int. Ed. 51 (2012) 12124–12127.
[25] M.J. Ju, J.C. Kim, H.J. Choi, I.T. Choi, S.G. Kim, K. Lim, J. Ko, J. Lee, I. Jeon, J. Baek, H.K. Kim, ACS Nano 7 (2013) 5243–5250.
[26] X.Y. Zhang, S.P. Pang, X. Chen, K.J. Zhang, Z.H. Liu, X.H. Zhou, G.L. Cui, RSC Adv. 3 (2013) 9005–9010.
[27] P. Karthika, N. Rajalakshmi, K.S. Dhathathreyan, J. Nanosci. Nanotechnol. 13 (2013) 1746–1751.
[28] R. Li, Z.D. Wei, X.L. Gou, W. Xu, RSC Adv. 3 (2013) 9978–9984.
[29] C.Z. Zhang, N. Mahmood, H. Yin, F. Liu, Y.L. Hou, Adv. Mater. 25 (2013) 4932–4937.
[30] J.R. He, Y.F. Chen, P.J. Li, Z.G. Wang, F. Qi, J.B. Liu, RSC Adv. 4 (2014) 2568–2572.
[31] Z.W. Liu, F. Peng, H.J. Wang, H. Yu, W.X. Zheng, J. Yang, Angew. Chem. Int. Ed. 50 (2011) 3257–3261.
[32] Y. Wang, Y.Y. Shao, D.W. Matson, J.H. Li, Y.H. Lin, ACS Nano 4 (2010) 1790–1798.
[33] X.L. Li, H.L. Wang, J.T. Robinson, H. Sanchez, G. Diankov, H.J. Dai, J. Am. Chem. Soc. 131 (2009) 15939–15944.
[34] T.V. Khai, H.G. Na, D.S. Kwak, Y.J. Kwon, H. Ham, K.B. Shim, H.W. Kim, J. Mater. Chem. 22 (2012) 17992–18003.
[35] Z.G. Wang, P.J. Li, Y.F. Chen, J.R. He, W.L. Zhang, O.G. Schmidt, Y.R. Li, Nanoscale (2014), http://dx.doi.org/10.1039/C3NR05061K.
[36] S. Eigler, C. Dotzer, A. Hirsch, Carbon 50 (2012) 3666–3673.
[37] W.J. Si, X.Z. Wu, J. Zhou, F.F. Guo, S.P. Zhuo, H.Y. Cui, W. Xing, Nanoscale Res. Lett. 8 (2013) 247.
[38] R. Liu, F.P. Shen, H.Y. Ding, J. Lin, W. Gu, Z. Cui, T. Zhang, J. Micromech. Microeng. 23 (2013) 065027.
[39] Q.G. He, Q. Li, S. Khene, X.M. Ren, F.E. Lopez-Suarez, D. Lozano-Castello, A. Bueno-Lopez, G. Wu, J. Phys. Chem. C 117 (2013) 8697–8707.
[40] K. Parvez, S.B. Yang, Y. Hernandez, A. Winter, A. Turchanin, X.L. Feng, K. Mullen, ACS Nano 6 (2012) 9541–9550.
[41] C.V. Rao, C.R. Cabrera, Y. Ishikawa, J. Phys. Chem. Lett. 1 (2010) 2622–2627.
[42] T. Ikeda, M. Boero, S. Huang, K. Terakura, M. Oshima, J. Ozaki, J. Phys. Chem. C 112 (2008) 14706–14709.
[43] R.A. Sidik, A.B. Anderson, N.P. Subramanian, S.M. Kumaraguru, B.N. Popov, J. Phys. Chem. B 110 (2006) 1787–1793.
[44] C.E. Banks, T.J. Davies, G.G. Wildgoose, R.G. Compton, Chem. Commun. (2005) 829–841.
[45] W.J. Yuan, Y. Zhou, Y.R. Li, C. Li, H.L. Peng, J. Zhang, Z.F. Liu, L.M. Dai, G.Q. Shi, Sci. Rep. 3 (2013) 2248.
[46] Z. Yang, Z. Yao, G.F. Li, G.Y. Fang, H.G. Nie, Z. Liu, X.M. Zhou, X.A. Chen, S.M. Huang, ACS Nano 6 (2012) 205–211.
[47] P.H. Matter, L. Zhang, U.S. Ozkan, J. Catal. 239 (2006) 83–96.